Journal of Materials Chemistry C

PAPER

View Article Online
View Journal | View Issue

Cite this: J. Mater. Chem. C, 2015, 3, 5783

Effective blocking of the molecular aggregation of novel truxene-based emitters with *spiro*bifluorene and electron-donating moieties for furnishing highly efficient non-doped blue-emitting OLEDs†

Chunliang Yao,[a] Yue Yu,[b] Xiaolong Yang,[a] Huiming Zhang,[a] Zuan Huang,[a] Xianbin Xu,[a] Guijiang Zhou,*[a] Ling Yue*[a] and Zhaoxin Wu*[b]

Received 12th April 2015,
Accepted 6th May 2015

DOI: 10.1039/c5tc01018g

www.rsc.org/MaterialsC

Several truxene-based blue fluorescent emitters bearing different functional moieties and peripheral *spiro*bifluorene groups have been successfully designed and synthesized. Through tuning the chemical structures and electronic characters of the functional moieties, both optimized molecular configuration and elevated highest occupied molecular orbital (HOMO) energy levels have been afforded to the truxene-based emitters, representing a new effective strategy for solving the problems of molecular aggregation and poor charge carrier injection/transport associated with the truxene-based blue emitters. Owing to the sophisticated strategy, the concerned emitters can furnish highly efficient non-doped blue-emitting OLEDs with a maximum current efficiency (η_L) of 7.41 cd A^{-1}, an external quantum efficiency (η_{ext}) of 4.33%, and a power efficiency (η_P) of 6.79 lm W^{-1}, representing the state-of-the-art EL efficiencies ever achieved by the truxene-based blue emitters. All promising results will not only show the great potential of the concerned truxene-based blue fluorescent emitters in the field of OLEDs, but also furnish valuable clues for developing high-performance truxene-based emitters.

Introduction

Blue fluorescent (singlet) emitters occupy a critical position in the field of organic light-emitting diodes (OLEDs) which have shown great potential in developing next generation flat-panel displays and energy-saving solid-state lighting sources, since both full-color display and white-light lighting will require blue emitters to fulfill three primary colors, *i.e.* red (R), green (G), and blue (B).[1–4] For the lighting purpose, the blue fluorescent emitters can also be employed to combine with orange (O) emitters to produce white light through O–B complementary colors in simplified device structures.[5–7] Through replacing the unstable phosphorescent (triplet) counterparts, blue fluorescent emitters can be used to construct white OLEDs (WOLEDs) to both guarantee high electroluminescent efficiencies *via* harnessing their unemissive triplet excitons by the long-wavelength triplet emitters and furnishing longer device life expectancy.[8,9] Besides these critical functions, a blue fluorescent emitter can also be utilized to generate light of long wavelength by an energy cascade to a suitably emissive dopant. However, the progress in blue OLEDs is lagged far behind the analogs of green and red due to the difficulty in developing blue-emitting materials with a high efficiency, color purity, and long lifetime.[9–11] Hence, searching high performance blue emitters definitely represents very crucial research lines in the field of OLEDs.

With the continuous efforts from the concerned researchers, various kinds of blue fluorescent emitters based on fluorene,[12–14] carbazole,[15,16] anthracene,[17,18] styrylarylene,[19] pyrene,[20,21] triphenylene,[22,23] biphenyl[24] and quinoline[25] derivatives have been developed to fabricate efficient blue OLEDs. From the structural diversity of the blue fluorescent emitters and their encouraging EL performance, it can be clearly seen that developing new chemical structures should be the most feasible way to cope with the problems in searching blue-emitting materials with a high EL performance.

[a] MOE Key Laboratory for Nonequilibrium Synthesis and Modulation of Condensed Matter, State Key Laboratory for Mechanical Behavior of Materials, and Institute of Chemistry for New Energy Materials, Department of Chemistry, Faculty of Science, Xi'an Jiaotong University, Xi'an 710049, P. R. China. E-mail: zhougj@mail.xjtu.edu.cn, heartstar@mail.xjtu.edu.cn; Fax: +86-029-82663914

[b] Key Laboratory of Photonics Technology for Information, Faculty of Electronic and Information Engineering, Xi'an Jiaotong University, Xi'an, 710049, P. R. China. E-mail: zhaoxinwu@mail.xjtu.edu.cn

† Electronic supplementary information (ESI) available: Synthetic scheme for the truxene-based emitters, synthetic details for the key intermediate compounds, and some EL data. See DOI: 10.1039/c5tc01018g

Truxene possesses a large π-conjugation system and multi reactive sites to afford diverse derivatives which can find applications in various fields.[26] Hence, besides the building-blocks aforementioned, truxene should also show great potential for developing novel blue fluorescent emitters due to the following facts: (1) truxene possesses a rigid planar skeleton with large π-conjugating structures, which can afford the indispensable characters to lead to a high fluorescent quantum yield (Φ_F), which is the most crucial parameter to furnish a high EL performance. (2) The energy-level for the S_1 states associated with the truxene π-conjugating system is high enough to produce fluorescence in the blue region. Unfortunately, the poor solubility and large steric hindrance make truxene difficult to modify and the large planar π-conjugating structures and structure of truxene will make it prone to aggregate to induce an undesired quenching effect.[27] Obviously, these characters will disfavor the truxene application in OLEDs. In order to cope with these problems, many truxene derivatives have been developed. The luminescent star-shaped conjugates with truxene as either the core[28–30] or the arms[31] have been prepared. The truxene-based oligomers and polymers have also been developed as light-emitting materials.[32,33] With truxene as the core or/and dendrons, novel luminescent dendrimers have been obtained.[34–36] In all of these truxene-based luminescent materials, long alkyl groups are typically introduced into the three internal bridging sp^3 hybrid carbon atoms of the truxene units with the aim of both enhancing good solubility and blocking effectively aggregation of these emissive molecules.[34,37,38] With all these improving strategies, the truxene-based luminescent molecules can exhibit a high fluorescent quantum yield (Φ_P).[29,39] Restraining the aggregation of the light-emitting truxene derivatives should be crucial for their application in blue-emitting OLEDs with a high color quality. Despite that doping can solve the aggregation problem of the blue emitters, a doped emitting layer (EML) in OLEDs will both show the susceptibility of undesired phase separation which will decrease the lifetime of the concerned devices and complicate device fabrication.

Despite many light-emitting truxene-based materials have been developed for various applications,[40–44] the ones applied in OLEDs as emitters are in limited number.[30,35,45,46] The first star-shaped truxene-based blue emitting can show a current efficiency (η_L) of 0.60 cd A^{-1}.[45] The truxene-based blue emitters with anthracene-based arms can show a maximum η_L of 2.98 cd A^{-1}.[30] Some novel truxene derivatives with sophisticated 3D configuration can bring narrow blue EL spectra with a maximum external quantum efficiency (η_{ext}) of 2.9%.[46] Recently, the star-shaped truxene-based blue emitter can bring a maximum η_L of 5.3 cd A^{-1}.[35] Despite these encouraging results, the concerned devices still show an inferior EL performance with respect to the blue-emitting OLEDs prepared by vacuum-deposition with other blue emitters.[47] However, the solution strategy has afforded a convenient and low-cost method to construct OLEDs. Hence, it is really necessary to develop novel truxene-based blue emitters. So, along this respect, several truxene derivatives bearing different functional moieties and peripheral *spiro*bifluorene groups have been successfully designed and prepared to furnish highly efficient solution-processed blue OLEDs. The concerned results should provide valuable information for designing highly efficient blue fluorescent emitters.

Experimental section

General information

All commercially available starting materials were used directly with no further purification. The solvents were carefully dried prior to use. All reactions were monitored using thin-layer chromatography (TLC) purchased from Merck & Co., Inc. Flash column chromatography and preparative TLC were made from silica gel bought from Shenghai Qingdao (200–300 mesh). ^{1}H NMR, ^{13}C NMR and ^{31}P NMR spectra were recorded in $CDCl_3$ on a Bruker Avance 400 MHz spectrometer and chemical shifts were referenced to the solvent residual peak at δ 7.26 for ^{1}H and 77.0 for ^{13}C, respectively. Elemental analyses were performed on a Flash EA 1112 elemental analyzer. The thermal gravimetric analysis (TGA) and differential scanning calorimetry (DSC) data were collected on a NETZSCH STA 409C instrument and a NETZSCH DSC 200 PC unit, respectively. UV-vis absorption spectra were measured at room temperature on a Shimadzu UV-2250 spectrophotometer. Emission spectra and lifetimes of these compounds were recorded on an Edinburgh Instruments Ltd (FLSP920) fluorescence spectrophotometer using the software package provided by Edinburgh Instruments. The fluorescent quantum yields (Φ_F) were determined in CH_2Cl_2 solutions at 298 K against quinine sulphate standard (Φ_P = 0.56).[48] Cyclic voltammetry was performed using a Princeton Applied Research model 273A potentiostat at a scan rate of 100 mV s^{-1}. All experiments were carried out in a three-electrode compartment cell with a Pt-sheet counter electrode, a glassy carbon working electrode, and a Pt-wire reference electrode. The supporting electrolyte used was 0.1 M $[n\mathrm{Bu_4N}]BF_4$ solution in acetonitrile. The concentration for all the samples was set at *ca.* 1.0 mM in acetonitrile. The onset oxidation (E_{po}) potentials were used to determine the HOMO energy levels using the equation $E_{HOMO} = -(E_{po} + 4.8)$ eV, which was calculated using the internal standard ferrocene value of −4.8 eV with respect to the vacuum.[49] The LUMO energy level was determined by the HOMO–LUMO gap (E_g) with the equation $E_{LUMO} = E_{HOMO} + E_g$. Fast atom bombardment (FAB) mass spectra were recorded on a Finnigan MAT SSQ710 system.

OLED fabrication and measurements

The pre-cleaned ITO glass substrates were treated with ozone for 20 min. Then, the PEDOT:PSS was deposited on the surface of ITO glass using a spin-coating method to form a 40 nm-thick hole-injection layer which was treated at 120 °C for 30 min in the air. The emitting layer (40 nm) was obtained by spin-coating a chlorobenzene solution of each corresponding emitters. The ITO glass was dried in a vacuum oven at 50 °C for 15 min and transferred to the deposition system for organic and metal deposition. TPBi (40 nm), LiF (1 nm) and Al cathodes (100 nm) were successively evaporated at a base pressure less than 10^{-6} Torr. The EL spectra and CIE coordinates were measured using

a PR650 spectra colorimeter. The *J–V–L* curves of the devices were recorded using a Keithley 2400/2000 source meter and the luminance was measured using a PR650 Spectra Scan spectrometer. All the experiments and measurements were carried out under ambient conditions.

Computational details

Geometrical optimizations were conducted using the popular B3LYP functional theory. The basis set used for C, H, N, and S atoms was 6-31G(d,p).[50,51] All calculations were carried out by using the Gaussian 09 program. In the vertical excitation energy calculation, all excited states were obtained using TD-DFT in the adiabatic approximation, using the same functional and basis set. A projection of the deformation in the relaxed excited-state onto the vibrational eigenvectors defined the Huang–Rhys factor S_j for each vibrational mode $\hbar\omega_j$. As well, the vibrational frequency ($\hbar\omega_j$) and the normal mode displacements (ΔQ_j) for each normal mode are calculated using the DUSHIN program.[52]

Results and discussion

Synthesis

The chemical structures of the designed truxene-based molecules are shown in Fig. 1. Their synthetic details have been presented in Scheme 1 and ESI.† All the target molecules are developed from truxene prepared from 3-phenylpropionic acid. In order to afford the processability to the blue emitters, the *n*-hexyl groups have been attached to the sp^3 hybrid carbon atoms of the truxene core **Tr-C**, which was converted into **Tr-CBr** with a high yield (*ca.* 93%) through the reaction with bromine in CH_2Cl_2 (Scheme 1). The blue emitter **Tr1** was obtained through the Suzuki cross-coupling reaction between **Tr-CBr** and 9,9′-*spiro*bifluoren-7-ylboronic acid. The other blue emitters **Tr2–Tr4** have been prepared in three steps of reaction. Firstly, through the Suzuki cross-coupling reaction with corresponding arylboronic acid, **Tr-CBr** can be transferred into intermediate compounds **Tr-Ar1–Tr-Ar3**. Secondly, the compounds **Tr-Ar1–Tr-Ar3** can react with NBS to form **Tr-ArBr1–Tr-ArBr3**. Finally, the target molecules **Tr2–Tr4** have been successfully prepared using the Suzuki cross-coupling reaction

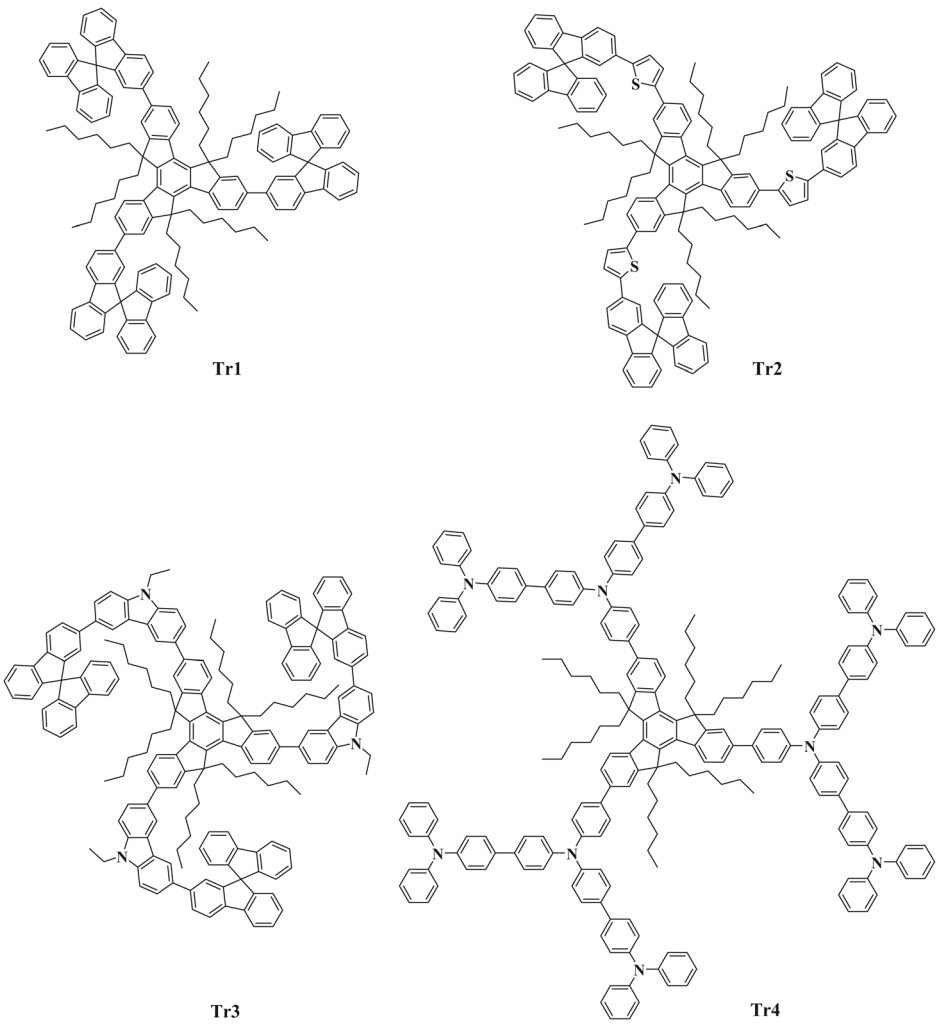

Fig. 1 The chemical structures of the truxene-based compounds.

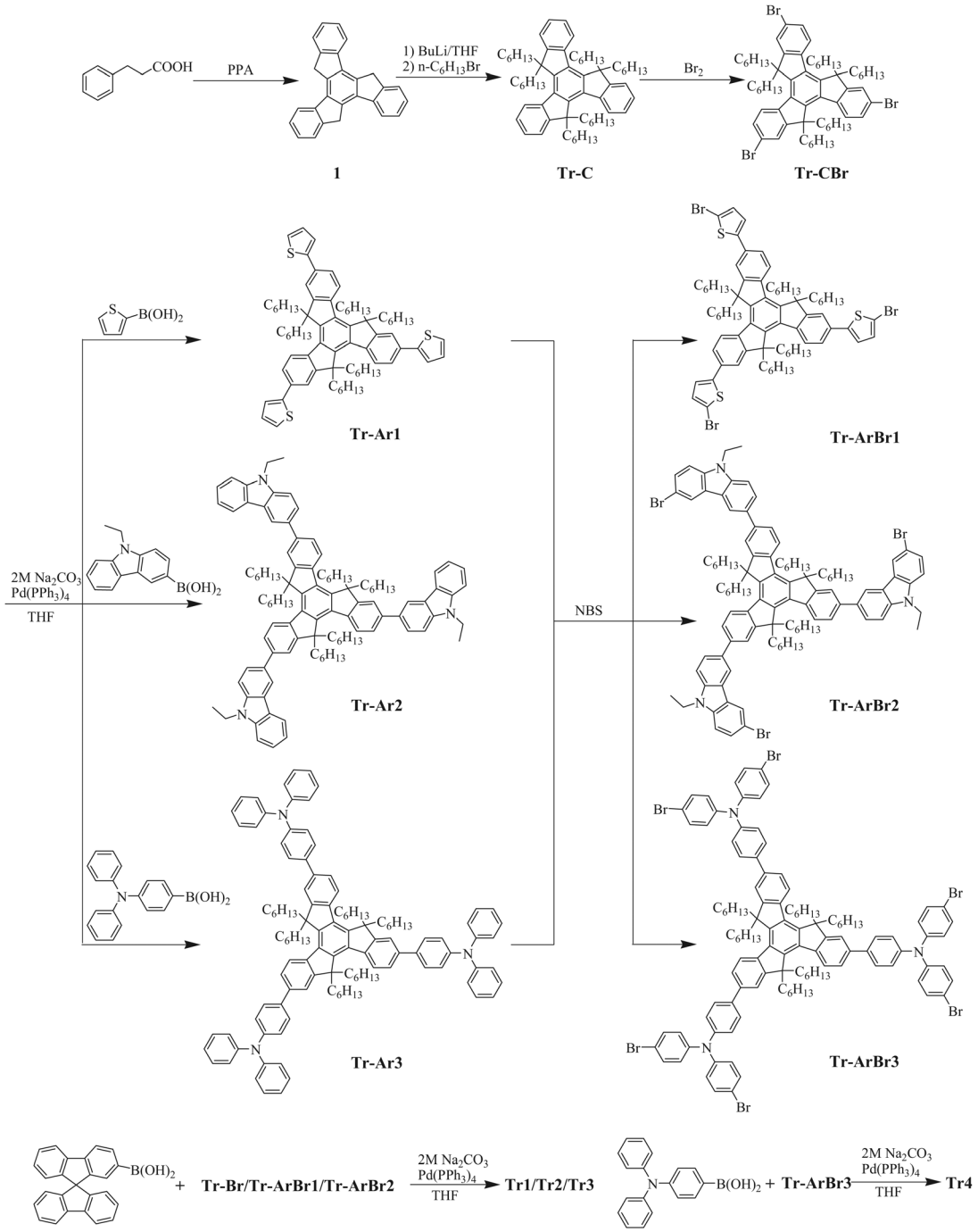

Scheme 1 Synthetic procedures for the truxene-based compounds.

in good yield (Scheme 1). Owing to their good solubility, all the truxene-based compounds can be purified by silica chromatography to be obtained as white or light yellow powder with high purity. Their well-defined chemical structures have been confirmed by nuclear magnetic resonance (NMR) (Fig. S1, ESI†), mass spectrometry (MS) (Fig. S2, ESI†), and elemental analysis.

Thermal and photophysical properties

The thermal characters of the truxene-based compounds have been characterized by thermal gravimetric analysis (TGA) and differential scanning calorimetry (DSC) with a scanning rate of 10 °C min^{-1} under a nitrogen atmosphere (Table 1 and Fig. S3, ESI†). The TGA results indicate that these compounds show excellent thermodynamic stability, with the 5% weight-reduction temperature ($\Delta T_{5\%}$) ranging from 396 to 421 °C. In addition, the DSC traces of the compounds revealed their high glass-transition temperatures (T_g) in the range from 151 to 178 °C and no crystallizing processes had been observed, suggesting the good morphological stability of the blue emitters. The excellent thermal properties associated with the truxene-based

Table 1 Photophysical and thermostability data for the truxene-based blue emitters

Compound	Absorption λ_{abs} [a] (nm)	Emission λ_{em} [b] (nm) solution	Emission λ_{em} [c] (nm) film	Φ_F [d] solution/film	τ_F [e] (ns)	$\Delta T_{5\%}/T_g$ (°C)
Tr1	228 (5.14), 264 (4.74), 296 (4.72), 308 (4.84), 342 (5.17)	380, 400, 420 sh	406, 426, 466	0.76/0.39	2.11	410/169
Tr2	230 (5.26), 296 (4.61), 308 (4.74), 392 (5.38)	432, 460, 489 sh	442, 466	0.59/0.45	0.70	396/178
Tr3	228 (5.29), 262 (5.09), 308 (5.24), 326 (5.29), 338 (5.28)	388, 406	397, 411	0.47/0.38	3.91	421/163
Tr4	232 (5.18), 304 (5.21), 370 (5.49)	447	432	0.58/0.49	1.66	420/151

[a] Measured in CH_2Cl_2 at a concentration of 10^{-6} M at 298 K, and log ε values are shown in parentheses. [b] Measured in CH_2Cl_2 at a concentration of 10^{-6} M, λ_{ex} = 334 nm. [c] Maximum emission wavelength measured in a film state, λ_{ex} = 334 nm. [d] Fluorescence quantum yields (Φ_F) were measured in CH_2Cl_2 using quinine sulfate in 1.0 M H_2SO_4 as the standard (Φ_F = 0.56), λ_{ex} = 334 nm. Φ_F for the solid film is obtained by an integrating sphere with λ_{ex} = 334 nm. [e] Measured in degassed CH_2Cl_2 solutions at a concentration of *ca.* 10^{-6} M, and the excitation wavelength was set at 334 nm for all the samples at 298 K.

molecules will guarantee the stabilities of the OLEDs based on them.

The UV-vis absorption spectra of the truxene-based molecules in solution are shown in Fig. 2a and the corresponding data are listed in Table 1. The high-energy absorption bands at around 230 nm should be induced by the absorption of the discrete aromatic units constructing the molecular skeletons. The sharp absorption band at *ca.* 308 nm can be ascribed to the absorption of the truxene core.[32] The strong absorption bands at a longer wavelength region from *ca.* 330 nm to 390 nm are assigned to the absorption transitions from the whole π-conjugation systems of the molecular skeletons of **Tr1–Tr4**. The UV-vis spectra of the truxene-based molecules in the neat film have also been measured (Fig. 2b). Compared with those in solution (Fig. 2a), the emission bands of these truxene-based molecules have been broadened, which have been observed in other truxene-based emitters.[38] However, the absorption maxima of **Tr1–Tr4** in the solid film just exhibit a slightly red-shift (Fig. 2). The molecules **Tr2** and **Tr4** exhibit obvious bathochromic shift in their predominant absorption band with respect to that of **Tr1** (Fig. 2). Notably, despite bearing a thiophene unit with small conjugation, **Tr2** can even possess lower absorption energy compared with **Tr4**. However, **Tr1** and **Tr3** show a very similar absorption onset (Fig. 2).

As aforementioned, the predominant absorption bands of these truxene-based molecules come from the transition of their expanded π-conjugation systems, which can be greatly affected by the molecular geometries. In order to interpret their absorption behaviors, the optimized molecular geometries together with the patterns of the frontier molecular orbitals (MOs) have been obtained by theoretical calculations using the DFT//B3LYP/6-31G(d,p) level with the Gaussian 09 program (Fig. 3). From the molecular geometry of **Tr2**, it can be seen clearly that the twisted angle of the thiophene unit between the truxene-core and peripheral *spiro*bifluorene blocks is *ca.* 28–29°, which is noticeably smaller than that between the truxene-core and peripheral *spiro*bifluorene blocks in **Tr1** (*ca.* 38°) (Fig. 3). This result indicates that the thiophene unit can effectively extend π-conjugation across the truxene-core and the peripheral groups to form large conjugation in **Tr2**, which will facilitate the absorption transition. Hence, the dominant absorption band assigned to the absorption transition in **Tr2** exhibits bathochromic shift with regard to that of **Tr1** (Fig. 2). In **Tr4**, the inner triphenylamine (TPA) unit shows a twisted angle of *ca.* 36–38° between the truxene-core and peripheral TPA groups (Fig. 3), indicating the poor π-conjugation extending the ability of the inner TPA units in **Tr4**. Why does **Tr4** still show bathochromic shift in its UV-vis absorption with respect to **Tr1** as aforementioned (Fig. 2)? From the MO patterns of **Tr4**, it can be concluded that the absorption transition of **Tr4** exhibits obvious intra-molecular charge transfer characters from the electron-donating TPA groups

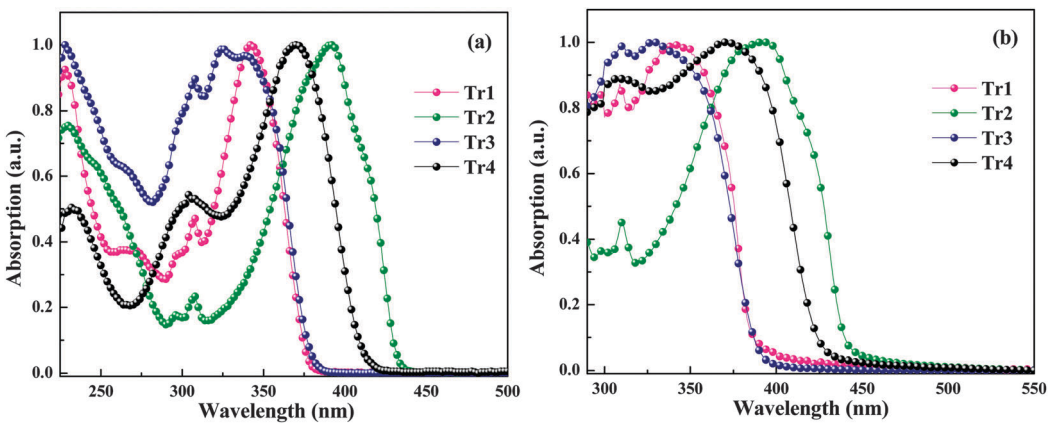

Fig. 2 The UV-vis absorption spectra of truxene-based compounds. (a) CH_2Cl_2 solution; (b) thin neat film.

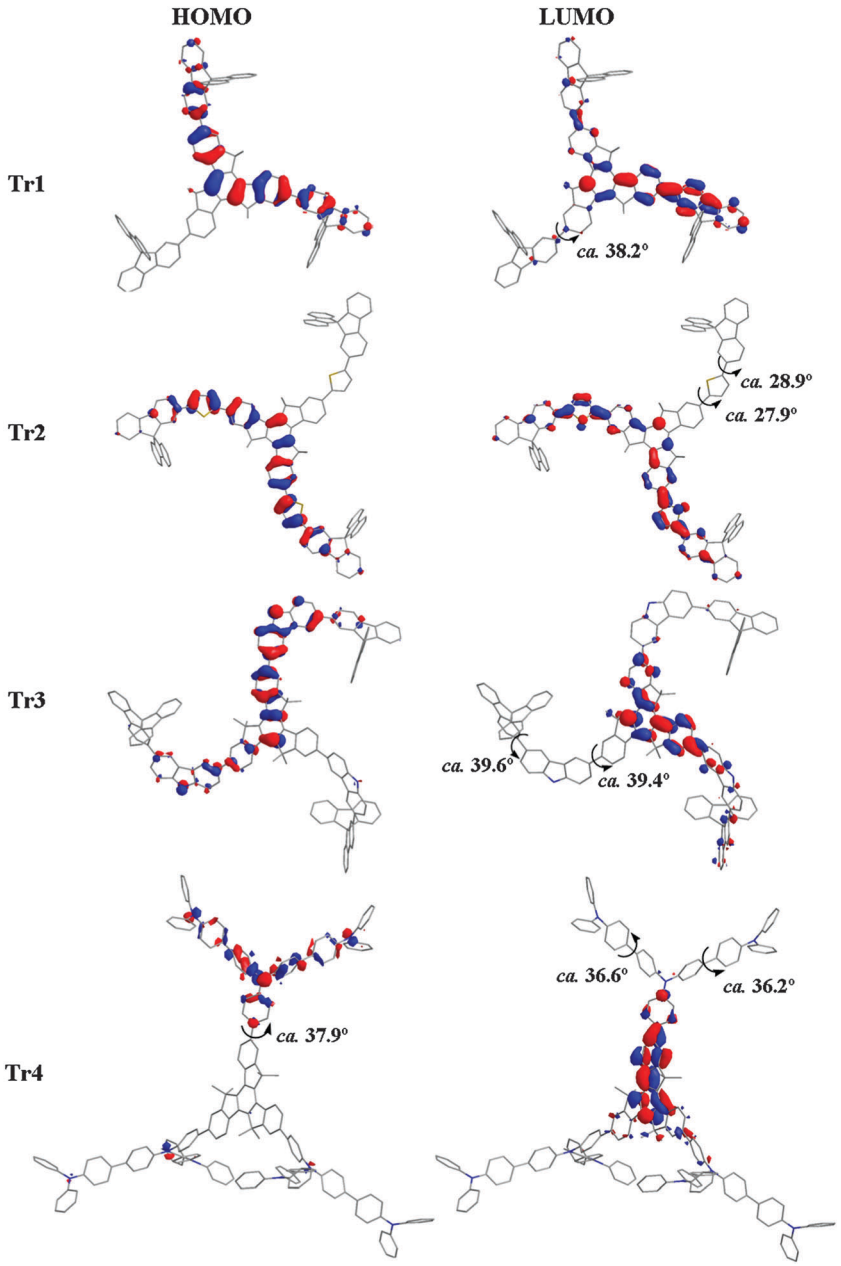

Fig. 3 The HOMO (left) and LUMO (right) patterns of the truxene-based compounds.

to the truxene-core (Fig. 3). Clearly, the molecular geometry of **Tr4** will show a trivial influence on its transition process. In contrast, the strong electron-donating ability associated with the TPA groups will promote the transition process in **Tr4**. Thus, **Tr4** can show bathochromic shift in its UV-vis absorption with regard to **Tr1**. Due to the effective conjugation interruption from the 3,6-carbazole substitution mode,[53–55] the carbazole unit in **Tr3** cannot extend the π-conjugation from the truxene-core to the peripheral *spiro*bifluorene blocks. As a result, **Tr1** and **Tr3** show very similar low-energy absorption bands (Fig. 2).

Fig. 4 illustrates the PL spectra of the truxene-based compounds in both CH_2Cl_2 solution and neat films. Except for **Tr4**, all compounds show two major emission peaks in CH_2Cl_2 solution, which can be assigned to the 0–0 and 0–1 singlet state transitions.[56] The shoulder emission peaks *ca.* 420 nm for **Tr1** and 489 nm for **Tr2** should come from the 0–2 transition. All the compounds exhibit major emission bands before 470 nm. Thus, they can be regarded as blue fluorescent emitters. The lifetimes associated with the blue-emitting bands are in the order of nanosecond (Table 1). It is well accepted that the LUMO ← HOMO transition typically corresponds with the lowest energy transition to form the first excited states, *i.e.* S_1 states for fluorescent emitters, leading to the emission of the luminescent materials by their radiative decay. Hence, the LUMO and HOMO patterns for **Tr1**, **Tr2**, **Tr3** and **Tr4** have been obtained by the DFT calculation (Fig. 3). The S_1 states should

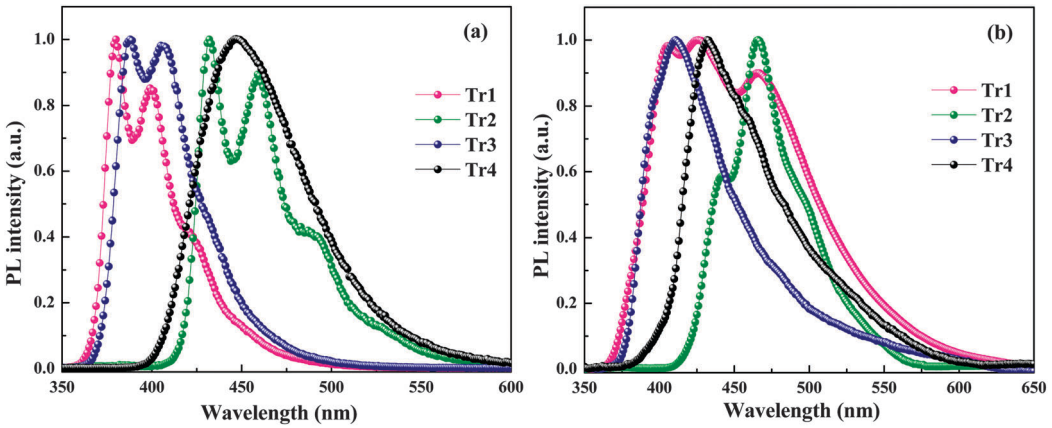

Fig. 4 The photoluminescence (PL) spectra of the truxene-based blue emitters at 298 K. (a) CH_2Cl_2 solution; (b) thin neat film.

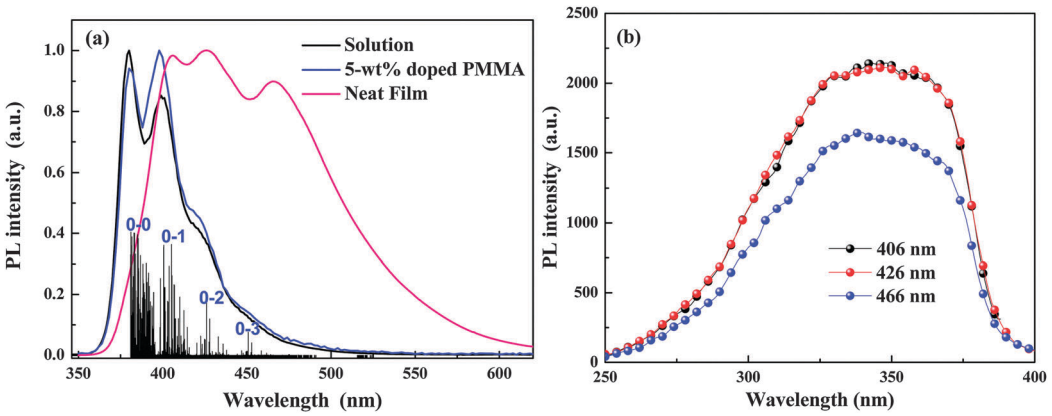

Fig. 5 (a) The PL spectra of **Tr1** in different states together with the calculated discrete vertical vibronic transitions (vertical columns); (b) excitation spectra of different emission bands in the solid film of **Tr1**.

response the fluorescence of these blue emitters. Thus, the LUMO ← HOMO transitions for **Tr1**, **Tr2**, **Tr3** and **Tr4** have been employed to interpret their emission behaviors. From the MO patterns for **Tr1**, **Tr2** and **Tr3**, it can be seen clearly that their LUMO ← HOMO transitions show obvious π–π* characters (Fig. 3). Thus, the PL spectra for **Tr1**, **Tr2** and **Tr3** all exhibit an obvious structured line-shape (Fig. 4a). Differently, LUMO ← HOMO transition for **Tr4** shows intra-molecular charge transfer character (*i.e.* from the triphenylamine moiety to the truxene core) features (Fig. 3). As a result, the PL spectrum of **Tr4** displays structureless features (Fig. 4a). Owing to the fact that the low-energy absorption bands of **Tr2** and **Tr4** locate in the longer wavelength region than those of **Tr1** and **Tr3** (Fig. 2), **Tr2** and **Tr4** possess longer emission wavelength than that of **Tr1** and **Tr3** (Fig. 4a and Table 1). The PL spectra in the solid film display different patterns compared with that in solution, especially for **Tr1**–**Tr3** (Fig. 4). This result can be ascribed to the self-absorption due to the broadening of the absorption band which will enhance the overlapping between absorption and emission bands in the solid film.

The PL spectra of the neat films with a thickness of *ca.* 100 nm for these truxene-based compounds have also been obtained (Fig. 4b). The dominant emission peak of **Tr1** in the neat film shows an obvious red-shift *ca.* 26 nm as compared with that in solution (Fig. 4 and Table 1). Furthermore, a new emission band at *ca.* 466 nm appears (Fig. 4 and Table 1). Compared with its PL spectrum in solution (Fig. 4a), the emission bands at 406 and 426 nm in the film of **Tr1** can be easily assigned to the 0–0 and 0–1 vibronically-resolved transitions (Fig. 4b). In order to find out the origin of the new emission band at *ca.* 466 nm in the **Tr1** film, the PL spectrum of the **Tr1** 5 wt% doped PMMA thin film with a thickness of *ca.* 100 nm has also been obtained to see whether the new emission band is induced by individual molecules of **Tr1** or the interaction among **Tr1** molecules (Fig. 5a). The PL maxima of the **Tr1** doped PMMA film are almost identical to those in the PL spectrum of the **Tr1** solution (Fig. 5a). However, no emission band at *ca.* 466 nm has been detected for the **Tr1** doped PMMA film (Fig. 5a). Clearly, the new emission band at *ca.* 466 nm should be induced by the multi-molecular behavior of **Tr1**. It should come from the aggregation of the **Tr1** molecules. In addition, the substantial red-shift effect in the solid film for **Tr1** also indicated the molecular aggregation according to the reported data.[32] In order to support this conclusion, various discrete vibronic transitions contributing to the PL spectra have been calculated using vibrational progressions (Fig. 5a).[57]

The theoretical calculations show excellent agreement with the experimental results from the PL spectra of both the solution and doped PMMA film of **Tr1**, indicating the validity of the calculation method. From solution to neat film, both the 0–0 and 0–1 emission peaks red-shift *ca.* 26 nm. However, wavelength margin between the new emission band (*ca.* 466 nm) in the neat film of **Tr1** and the 0–2 emission peak *ca.* 420 nm for **Tr1** in both solution and doped PMMA film is *ca.* 46 nm. Furthermore, the theoretical results indicate that the 0–2 emission peak for **Tr1** should be much weaker than the 0–0 and 0–1 emission peaks. However, the new emission band (*ca.* 466 nm) in the neat film of **Tr1** exhibits nearly the same intensity of the 0–0 and 0–1 emission peaks. All these results indicate that the new emission band at *ca.* 466 nm in the neat film of **Tr1** might not come from the high-frequency vibrational modes. Even there is contribution from the 0–2 emission to the PL band at *ca.* 466 nm in the neat film of **Tr1**, the contribution should also in subordinate place due to the low transition possibility (Fig. 5a). The excitation spectra of different emission bands of the **Tr1** solid film have been measured (Fig. 5b). In Fig. 5b, the new emission band at *ca.* 466 nm shows a very similar excitation spectrum to the other two emission bands, which also exhibit the inherent character of the excimer emission due to the molecular aggregation.[58] Φ_Fs in both solution and solid film of these truxene-based compounds should also indicate the molecular aggregation in **Tr1** (Table 1). From solution to solid film, **Tr1** exhibits the highest reduction of Φ_F (*ca.* 49%) compared with other analogs (*ca.* 24% for **Tr2**, 19% for **Tr3** and 16% for **Tr4**), which can be ascribed to the quenching effect induced by molecular aggregation in **Tr1**. Hence, the *n*-hexyl groups and *spiro*bifluorene blocks might not effectively block the molecular aggregation among the **Tr1** molecules.

It has been accepted that introducing long alkyl chains can effectively block the aggregation the concerned truxene derivatives.[37,38] In some compounds, there is only a very slight red-shift effect in PL maxima can be observed in going from solution to solid film. However, from solution to neat film, a pronounced red-shift of *ca.* 23 nm in some truxene derivatives with long alkyl chains has been ascribed to the molecular aggregation effect.[26,37] The truxene-based compound with both *n*-hexyl groups and six fluorene substituents still shows ability in blocking the molecular aggregation. The truxene derivatives with six *n*-hexyl groups and three oligo(*p*-phenylene) arms still show molecular aggregation indicated by the large red-shift effect of PL maxima in the solid film.[32] Thus, it seems that ability of the long alkyl chains in blocking the aggregation of the truxene derivatives can be influenced by the molecular structures. So, the molecular structure of **Tr1** might disfavor the blocking of molecular aggregation of the hexyl groups.

For **Tr2** and **Tr3**, the red-shift effect is *ca.* 10 and 5 nm for the major emission band on going from solution to neat film, respectively. However, the emission band at *ca.* 447 nm for **Tr4** in solution even shows a red-shift *ca.* 15 nm compared with that from its neat film. This result can be explained as follows: as aforementioned, the emissive excited states S_1 of **Tr4** possess obvious intra-molecular charge transfer characters, which will make them possess obvious polar characters. Accordingly, the polar excited states S_1 of **Tr4** will be stabilized in the polar solvent (such as CH_2Cl_2) to show a positive solvatochromism effect which can lead to an obvious red-shift of the emission band of the concerned molecules in the polar solvent (Fig. S4, ESI†). In order to eliminate the influence of the solvatochromism effect, the PL spectra of **Tr4** in low-polar toluene have been recorded. The PL maximum of the neat film of **Tr4** shows a very slight red-shift effect *ca.* 2 nm with respect to that in toluene (Fig. S4, ESI†). This result indicates that there is nearly no aggregation among the molecules of **Tr4**.

As aforementioned, the large planar skeleton of truxene typically induces serious molecular aggregation, which will impede the EL efficiency and color purity. Hence, the concerned researchers have done their best to block this undesired aggregation process associated with truxene. In this study, the *spiro*bifluorene and triphenylamine blocks have been introduced to fulfill the purpose, since *spiro*bifluorene possesses two fluorene units adopting perpendicular configuration and triphenylamine shows twisted propeller geometry. However, the molecules of **Tr1** still show aggregation in the neat film (Fig. 4b), indicating that the *n*-hexyl groups attached to the truxene core might not show enough ability in effectively coping with the molecular aggregation problem in this case. Clearly, the molecular aggregation should have tight relationship with the configuration of the concerned molecules. Hence, the molecular configurations have been optimized (Fig. 6). Despite the deviation from theoretical configuration, the actual molecules tend to adopt the optimized configurations since they represent the low-energy and stable states. From the molecular configuration of **Tr1**, it can be seen clearly that the *spiro*bifluorene moieties are located at one side of the truxene core (Fig. 6 and Fig. S5, ESI†), which will leave another side of the truxene core to pack with the other truxene core. Hence, the molecules of **Tr1** exhibit aggregation in the neat film (Fig. S5, ESI†). Through inserting a thiophene unit in between *spiro*bifluorene and truxene cores, **Tr2** should adopt more favorable configuration in blocking molecular aggregation due to the fact that one fluorene unit in *spiro*bifluorene moieties points to both sides of the truxene core. Thus, only 10 nm red-shift has been observed in the neat film of **Tr2** with respect to its solution despite its similar molecular "thickness" to that of **Tr1**. Owing to the large twist angle of *ca.* 40° between the peripheral groups and the truxene core (Fig. 3), the molecules of **Tr3** and **Tr4** possess much larger "thickness" (*ca.* 20.64 Å for **Tr3** and 25.96 Å for **Tr4**) compared with **Tr1** and **Tr2** (Fig. 6), which can effectively block the aggregation of the truxene core in **Tr3** and **Tr4**. Hence, a very slight red-shift effect has been detected for the emission maxima of the neat films for **Tr3** and **Tr4** as aforementioned (Table 1 and Fig. 4). The slight red-shift effect in PL maxima of their neat film indicates that the strategy employed in this study should represent a very effective strategy to overcome the problem of molecular aggregation associated with the truxene core. Importantly, all these results have clearly indicated that inserting different aromatic units in the arms of the branched truxene-based emitters can effectively alter the molecular configuration to block the undesired molecular aggregation effect. It can provide important information for

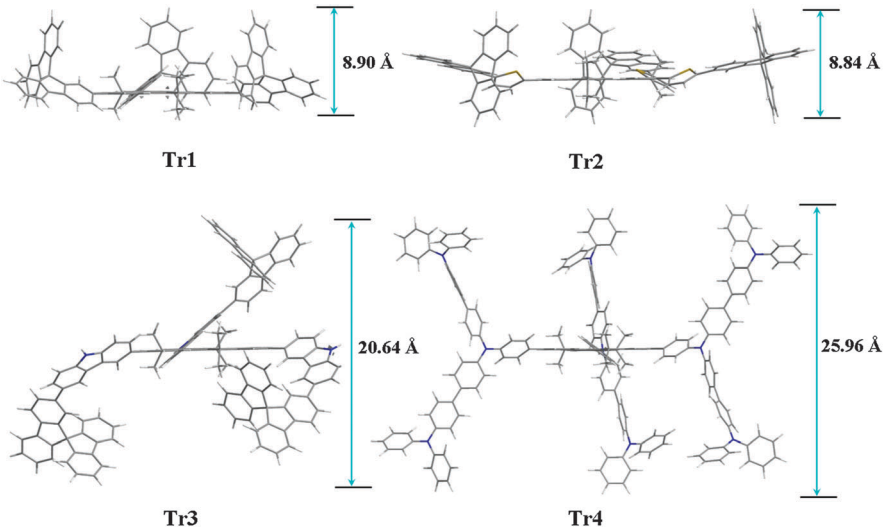

Fig. 6 The side-view of the optimized molecular configuration of the truxene-based compound. The *n*-hexyl groups have been replaced by the methyl group for both the calculation convenience and their little effect in blocking the molecular aggregation.

Table 2 Redox properties of the truxene-based compounds

Compound	E_{pa} [a] (V)	E_{po} [b] (V)	E_g^{opt} [c] (eV)	E_{HOMO} (eV)	E_{LUMO} (eV)
Tr1	0.93	0.77	3.28	−5.57	−2.29
Tr2	0.79	0.56	2.88	−5.36	−2.48
Tr3	0.69	0.47	3.27	−5.27	−2.00
Tr4	0.40, 0.59, 0.79	0.23	3.01	−5.03	−2.01

[a] Oxidation potential. [b] Onset oxidation potential. [c] Calculated from the absorption onset of the UV-vis absorption spectra.

the design and synthesis of truxene-based emitters free of molecular aggregation.

Electrochemical properties

The electrochemical properties of the truxene-based emitters have been characterized by cyclic voltammetry (CV) measurement calibrated with ferrocene as standard under a nitrogen atmosphere (Table 2 and Fig. S6, ESI†). Except for **Tr4**, all the compounds show a quasi-reversible oxidation wave with potential (E_{pa}) at 0.93 V for **Tr1**, 0.79 V for **Tr2** and 0.69 V for **Tr3**, respectively. However, the compound **Tr4** exhibits three quasi-reversible oxidation waves with E_{pa} of 0.40, 0.59, and 0.79 V. Compared with **Tr1**, the compounds **Tr2**, **Tr3** and **Tr4** display noticeably lower first oxidation potentials (Table 2), indicating their better hole injection ability. The lower E_{pa} for **Tr2** should benefit from the extended conjugation across the truxene core and the arms due to the small twisted angle between the thiophene units and both the truxene core and the *spiro*bifluorene moieties (Fig. 3), which will destabilize the HOMO level of **Tr2**. Differently, the reduced E_{pa} for **Tr3** and **Tr4** should be induced by the electron-donating property of the carbazole and triphenylamine moieties, since the conjugation in **Tr3** and **Tr4** cannot be effectively extended due to their twisted molecular configuration (Fig. 6). Owing to the stronger electron-donating ability of the triphenylamine unit than that of the carbazole group, **Tr4** can show the first E_{pa} as low as 0.23 V. The onset oxidation potentials (E_{po}) of these molecules have also been obtained to calculate the HOMO levels (E_{HOMO}): $E_{HOMO} = -(E_{po}^{ox} + 4.8)$ eV.[38] Based on the optical gap (E_g^{opt}) of these blue emitters, their LUMO levels (E_{LUMO}) can be obtained (Table 2). Clearly, **Tr2** possesses the lowest E_{LUMO}, which can be assigned to the fact that both the HOMO and LUMO locate on nearly the same area of **Tr2** (Fig. 3). Thus, it will facilitate LUMO ← HOMO transition and make the E_{LUMO} of **Tr2** closer to its E_{HOMO}.

Electroluminescent characterization

In order to investigate their electroluminescent characteristics, non-doped blue-emitting OLEDs have been constructed with these truxene-based emitters as emission layers. Due to their good solubility in common solvents such as CH_2Cl_2, toluene and chlorobenzene *etc.*, the concerned devices were easily fabricated with a solution-processing approach with the configuration of ITO/PEDOT:PSS (40 nm)/emitters (EML) (40 nm)/TPBi (40 nm)/LiF (1 nm)/Al (100 nm). Fig. 7 depicts the structure of the multi-layer OLEDs and the functional materials involved in the fabrication of the devices. The PEDOT:PSS layer was firstly deposited by spin-coating on the pre-cleaned ITO surface to form a hole-injection layer (HIL) for its HOMO level matching with that of ITO. The emission layer (EML) is deposited on the PEDOT:PSS layer by spin-coating the chlorobenzene solution of the concerned emitters. The 1,3,5-tris(1-phenyl-1*H*-benzo[*d*]imidazol-2-yl)benzene (TPBi) layer plays the role of both hole-blocking and electron-transporting, while LiF acts as an electron-injection layer.

When proper voltage was applied, except device A, all devices emit blue electroluminescence (Fig. 8). Compared with the PL spectrum of **Tr1** in both solution and neat film, the long-wavelength band at *ca.* 500 nm in the EL spectrum of device A should come from the molecular aggregation of **Tr1** as aforementioned. This has seriously affected the EL blue color quality by shifting the CIE coordinates towards the green region in the

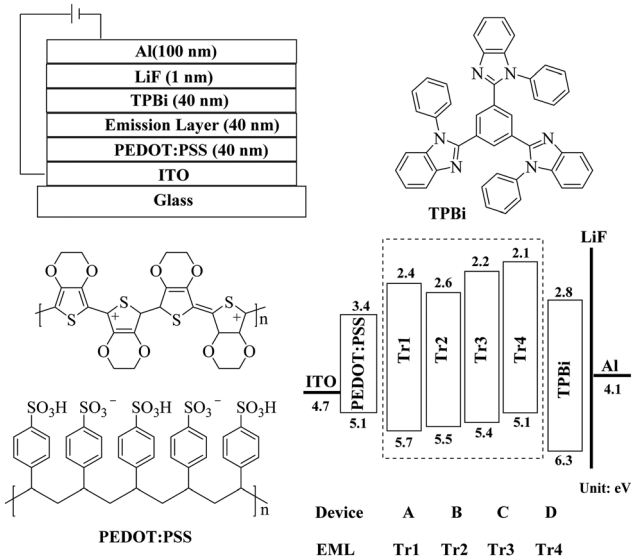

Fig. 7 The general configuration for OLEDs made from the truxene-based emitters and the chemical structures of the relevant compounds used in these devices.

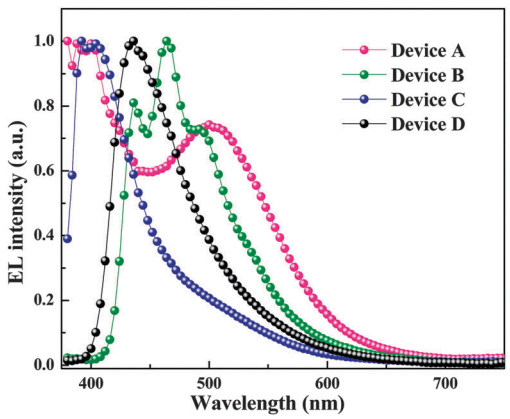

Fig. 8 The EL spectra of the OLEDs made from the truxene-based emitters at 9 V.

chromaticity diagram (Table 3). Hence, the EL emission from device A can be regarded as bluish-green color. Owing to the favorable configuration of **Tr2**, **Tr3**, and **Tr4** in blocking molecular aggregation, the concerned device can show EL spectra without long-wavelength EL bands induced by molecular aggregation (Fig. 8), maintaining the blue EL color. According to the CIE coordinates (Table 3), device B can show greenish-blue EL emission, while both devices C and D emit blue EL color. These results have clearly indicated the crucial role played by our molecular design strategy in relieving the molecular aggregation problem associated with the truxene-based emitters.

The current density (J)–voltage (V)–luminance (L) curves of the concerned devices are shown in Fig. 9, while the relationship between EL efficiencies and current density for the devices are presented in Fig. 10 and Fig. S7 (ESI†). Owing to the serious molecular aggregation of **Tr1** in the EML, device A shows very poor EL efficiencies (Table 3). In contrast, the other devices can exhibit much improved EL performances. The device B can furnish maximum EL ability with a maximum brightness (L_{max}) of 11 629 cd m^{-2} at 11.3 V, a peak external quantum efficiency (η_{ext}) of 1.68%, a current efficiency (η_L) of 3.88 cd A^{-1}, and a power efficiency (η_p) of 1.33 lm W^{-1}. Notably, devices C and D can even exhibit better EL performances compared with device B (Table 3). Device C can show a low turn-on voltage ($V_{turn\text{-}on}$) of 4.0 V, L_{max} of 5306 cd m^{-2} at 9.3 V, η_{ext} of 4.61%, η_L of 4.85 cd A^{-1}, and η_p of 2.71 lm W^{-1}. Encouragingly, device D can furnish even better EL performances with $V_{turn\text{-}on}$ of 2.8 V, L_{max} of 9461 cd m^{-2}, η_{ext} of 4.33%, η_L of 7.41 cd A^{-1}, and η_p of 6.79 lm W^{-1}. Even at a high luminance of 500 cd m^{-2}, device C/D can still show high EL efficiencies with η_{ext} of 4.40/3.96%, η_L of 4.62/6.77 cd A^{-1}, and η_p of 2.41/3.79 lm W^{-1} (Table 3 and Fig. 10). The good hole injection/transporting ability associated with the carbazole and triphenylamine units should benefit the improved EL performances of device C and D. Besides the contribution from its good hole injection/transporting ability, the admirable EL performance of **Tr4** can also be attributed to its proper HOMO level of *ca.* 5.08 eV, which is almost the same as that of PEDOT:PSS (*ca.* 5.1 eV). Thus, the hole injection from the PEDOT:PSS layer to EML of device D should be nearly barrier-free (Fig. 7). In addition, the energy barrier between the EML of device D and the hole-blocking layer (TPBi) is the largest (*ca.* 1.22 eV) (Fig. 7), which can effectively restrain the injected holes in the EML to combine with the injected electrons rather than drift the cathode and form current without combination. Hence, the charge recombination efficiency should be greatly improved to bring high EL efficiency for device D based on **Tr4**. From device A to device D, $V_{turn\text{-}on}$ decreases gradually, which can be ascribed to the continuous elevating of the HOMO levels from **Tr1** to **Tr4** to facilitate the hole injection to the EMLs

Table 3 The EL performance of the OLEDs made from the truxene-based fluorescent emitters

Device	$V_{turn\text{-}on}$ (V)	Luminance[a] (cd m^{-2})	η_{ext} (%)	η_L (cd A^{-1})	η_p (lm W^{-1})	λ_{max}[c] (nm)	CIE[c] (x,y)
A	6.5	821 (10.1)	0.52 (8.1)[a] 0.51[b]	1.13 (8.1)[a] 1.11[b]	0.44 (8.1)[a] 0.42[b]	388, 400, 500	(0.21, 0.30)
B	4.3	11 629 (11.3)	1.68 (9.1) 0.38	3.88 (9.1) 0.88	1.33 (9.1) 0.41	436, 464, 492	(0.18, 0.22)
C	4.0	5306 (9.3)	4.61 (5.7) 4.40	4.85 (5.7) 4.62	2.71 (5.5) 2.41	392, 404	(0.18, 0.15)
D	2.8	9461 (9.3)	4.33 (4.0) 3.96	7.41 (4.0) 6.77	6.79 (2.6) 3.79	436	(0.17, 0.15)

[a] Maximum values of the devices. Values in parentheses are the voltages at which data were obtained. [b] Values at 500 cd m^{-2}. [c] Values collected at 9 V.

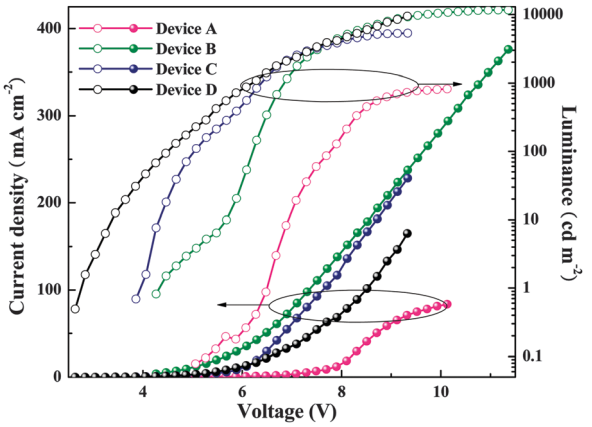

Fig. 9 The current density (*J*)–voltage (*V*)–luminance (*L*) curves of all the devices.

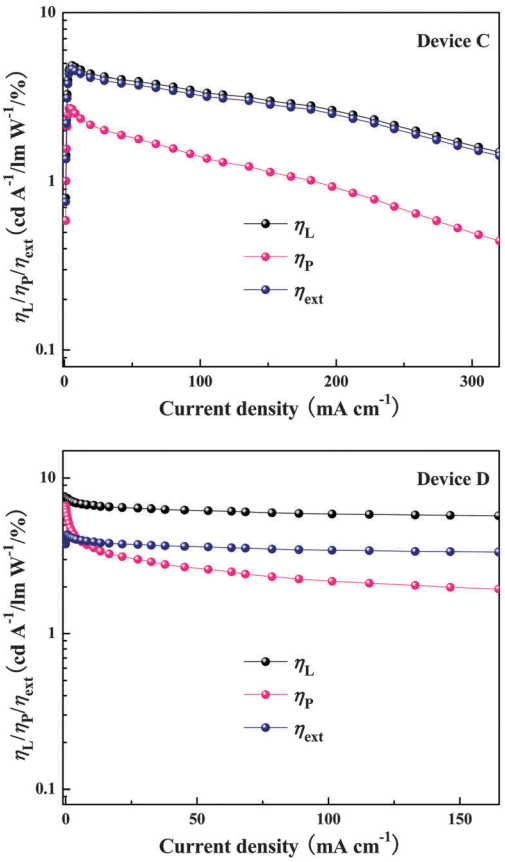

Fig. 10 The relationship between EL efficiencies and current density for the devices C and D.

in the concerned devices, indicating the advantage of employing functional moieties in developing truxene-based emitters. There are also some high-performance truxene-based emitters employed in OLEDs. Yang and coworkers have reported some truxene-based blue emitters that can achieve peak η_L of 4.01 cd A^{-1} and η_P of 3.60 lm W^{-1}.[38] Some truxene-based blue emitters with anthracene substituents can furnish η_L of 2.98 cd A^{-1} and η_P of 1.52 lm W^{-1}.[30] The deep-blue emitting OLEDs made from truxene-based dendrimers can exhibit high EL efficiencies with η_L of 5.3 cd A^{-1} and η_{ext} of 6.6%.[39] Compared with all these good documented results, the EL performances in this study have not only indicated the great potential of these novel truxene-based emitters in furnishing highly efficient blue-emitting OLEDs, but also shown the important value of the conception for molecular design in coping with the problems associated with truxene-based emitters.

Conclusion

Through introducing the *spiro*bifluorene unit and electron-donating moieties, such as thiophene, carbazole, and triphenylamine groups, four truxene-based blue emitters have been successfully developed with the optimized molecular configuration which can effectively block the undesired aggregation of the truxene core. Furthermore, good electron injection/transporting ability has been afforded to the blue fluorescent emitters by the electron-donating blocks. Benefiting from all these advantages of these truxene-based novel blue emitters, the concerned non-doped solution-processed blue-emitting OLEDs can furnish very high EL performances with $V_{turn\text{-}on}$ of 2.8 V, L_{max} of 9461 cd m^{-2}, η_{ext} of 4.33%, η_L of 7.41 cd A^{-1}, and η_p of 6.79 lm W^{-1}, which might represent the state-of-the-art performance for truxene-based blue-emitting OLEDs. All these encouraging data will not only show the great potential of these blue emitters, but also provide important information for design and synthesis of high-performance truxene-based fluorescent emitters.

Acknowledgements

This work was financially supported by Tengfei Project from Xi'an Jiaotong University, the Fundamental Research Funds for the Central Universities, The Program for New Century Excellent Talents in University, the Ministry of Education of China (NECT-09-0651), the Key Creative Scientific Research Team in Shaanxi Province (2013KCT-05), the China Postdoctoral Science Foundation (Grant no. 20130201110034), and the National Natural Science Foundation of China (no. 20902072). The financial support from the State Key Laboratory for Mechanical Behavior of Materials is also acknowledged.

References

1 M. R. Zhu and C. L. Yang, *Chem. Soc. Rev.*, 2013, **42**, 4963–4976.
2 Z. Ma, P. Sonar and Z. K. Chen, *Curr. Org. Chem.*, 2010, **14**, 2034–2069.
3 L. X. Xiao, Z. J. Chen, B. Qu, J. X. Luo, S. Kong, Q. H. Gong and J. J. Kido, *Adv. Mater.*, 2011, **23**, 926–952.
4 C. C. Tsou, H. T. Lu and M. Yokoyama, *J. Cryst. Growth*, 2005, **280**, 201–205.
5 T. Peng, Y. Yang, H. Bi, Y. Liu, Z. M. Hou and Y. Wang, *J. Mater. Chem.*, 2011, **21**, 3551–3553.
6 Y. B. Zhao, L. P. Zhu, J. S. Chen and D. G. Ma, *Org. Electron.*, 2012, **13**, 1340–1348.

7 J. Liu, Q. G. Zhou, Y. X. Cheng, Y. H. Geng, L. X. Wang, D. G. Ma, X. B. Jing and F. S. Wang, *Adv. Funct. Mater.*, 2006, **16**, 957–965.
8 G. Schwartz, M. Pfeiffer, K. Walzer and K. Leo, *Proc. Soc. Photo-Opt. Instrum. Eng.*, 2007, **6655**, J6550.
9 G. Schwartz, M. Pfeiffer, S. Reineke, K. Walzer and K. Leo, *Adv. Mater.*, 2007, **19**, 3672–3676.
10 X. Y. Cai, A. B. Padmaperuma, L. S. Sapochak, P. A. Vecchi and P. E. Burrows, *Appl. Phys. Lett.*, 2008, 92.
11 C. H. Yang, Y. M. Cheng, Y. Chi, C. J. Hsu, F. C. Fang, K. T. Wong, P. T. Chou, C. H. Chang, M. H. Tsai and C. C. Wu, *Angew. Chem., Int. Ed.*, 2007, **46**, 2418–2421.
12 N. Cho, B. K. Choi, H. Suh, J. J. Park, J. M. Kim and K. S. Lee, *J. Nanosci. Nanotechnol.*, 2010, **10**, 6925–6928.
13 S. L. Tao, Z. K. Peng, X. H. Zhang, P. F. Wang, C. S. Lee and S. T. Lee, *Adv. Funct. Mater.*, 2005, **15**, 1716–1721.
14 T. C. Chao, Y. T. Lin, C. Y. Yang, T. S. Hung, H. C. Chou, C. C. Wu and K. T. Wong, *Adv. Mater.*, 2005, **17**, 992–996.
15 Z. Q. Jiang, H. Q. Yao, Z. Y. Liu, C. L. Yang, C. Zhong, J. Qin, G. Yu and Y. Q. Liu, *Org. Lett.*, 2009, **11**, 4132–4135.
16 T. Peng, G. F. Li, Y. Liu, Y. Wu, K. Q. Ye, D. D. Yao, Y. Yuan, Z. M. Hou and Y. Wang, *Org. Electron.*, 2011, **12**, 1068–1072.
17 S. K. Kim, B. Yang, Y. Ma, J. H. Lee and J. W. Park, *J. Mater. Chem.*, 2008, **18**, 3376–3384.
18 Y. H. Kim, D. C. Shin, S. H. Kim, C. H. Ko, H. S. Yu, Y. S. Chae and S. K. Kwon, *Adv. Mater.*, 2001, **13**, 1690–1693.
19 K. S. Kim, Y. M. Jeon, J. W. Kim, C. W. Lee and M. S. Gong, *Dyes Pigm.*, 2008, **77**, 238–244.
20 F. Liu, W. Y. Lai, C. Tang, H. B. Wu, Q. Q. Chen, B. Peng, W. Wei, W. Huang and Y. Cao, *Macromol. Rapid Commun.*, 2008, **29**, 659–664.
21 C. Tang, F. Liu, Y. J. Xia, J. Lin, L. H. Xie, G. Y. Zhong, Q. L. Fan and W. Huang, *Org. Electron.*, 2006, **7**, 155–162.
22 P. Y. Chou, H. H. Chou, Y. H. Chen, T. H. Su, C. Y. Liao, H. W. Lin, W. C. Lin, H. Y. Yen, I. C. Chen and C. H. Cheng, *Chem. Commun.*, 2014, **50**, 6869–6871.
23 S. O. Kim, H. S. Jang, S. J. Lee, Y. K. Kim and S. S. Yoon, *Bull. Korean Chem. Soc.*, 2013, **34**, 2267–2270.
24 S. M. Kwon, K. H. Lee, S. J. Lee, Y. K. Kim and S. S. Yoon, *Mol. Cryst. Liq. Cryst.*, 2013, **584**, 103–112.
25 C. J. Tonzola, A. P. Kulkarni, A. P. Gifford, W. Kaminsky and S. A. Jenekhe, *Adv. Funct. Mater.*, 2007, **17**, 863–874.
26 F. Goubard and F. Dumur, *RSC Adv.*, 2015, 3521–3551.
27 X. Y. Cao, X. H. Liu, X. H. Zhou, Y. Zhang, Y. Jiang, Y. Cao, Y. X. Cui and J. Pei, *J. Org. Chem.*, 2004, **69**, 6050–6058.
28 S. C. Yuan, H. B. Chen, Y. Zhang and J. Pei, *Org. Lett.*, 2006, **8**, 5700–5704.
29 A. L. Kanibolotsky, R. Berridge, P. J. Skabara, I. F. Perepichka, D. D. C. Bradley and M. Koeberg, *J. Am. Chem. Soc.*, 2004, **126**, 13695–13702.
30 J. H. Huang, B. Xu, J. H. Su, C. H. Chen and H. Tian, *Tetrahedron*, 2010, **66**, 7577–7582.
31 X. F. Duan, J. L. Wang and J. Pei, *Org. Lett.*, 2005, **7**, 4071–4074.
32 W. B. Zhang, W. H. Jin, X. H. Zhou and J. Pei, *Tetrahedron*, 2007, **63**, 2907–2914.
33 X. Y. Cao, X. H. Zhou, H. Zi and J. Pei, *Macromolecules*, 2004, **37**, 8874–8882.
34 Y. Jiang, J. Y. Wang, Y. G. Ma, Y. X. Cui, Q. F. Zhou and J. Pei, *Org. Lett.*, 2006, **8**, 4287–4290.
35 L. Wang, Y. Jiang, J. Luo, Y. Zhou, J. H. Zhou, J. Wang, J. Pei and Y. Cao, *Adv. Mater.*, 2009, **21**, 4854–4858.
36 X. Y. Cao, W. B. Zhang, J. L. Wang, X. H. Zhou, H. Lu and J. Pei, *J. Am. Chem. Soc.*, 2003, **125**, 12430–12431.
37 X. Y. Cao, W. Zhang, H. Zi and J. Pei, *Org. Lett.*, 2004, **6**, 4845–4848.
38 Z. F. Yang, B. Xu, J. T. He, L. L. Xue, Q. Guo, H. J. Xia and W. J. Tian, *Org. Electron.*, 2009, **10**, 954–959.
39 A. L. Kanibolotsky, I. F. Perepichka and P. J. Skabara, *Chem. Soc. Rev.*, 2010, **39**, 2695–2728.
40 Y. Wang, G. Tsiminis, Y. Yang, A. Ruseckas, A. L. Kanibolotsky, I. F. Perepichka, P. J. Skabara, G. A. Turnbull and I. D. W. Samuel, *Synth. Met.*, 2010, **160**, 1397–1400.
41 Y. M. Sun, K. Xiao, Y. Q. Liu, J. L. Wang, J. Pei, G. Yu and D. B. Zhu, *Adv. Funct. Mater.*, 2005, **15**, 818–822.
42 L. Sanguinet, J. C. Williams, Z. Y. Yang, R. J. Twieg, G. L. Mao, K. D. Singer, G. Wiggers and R. G. Petschek, *Chem. Mater.*, 2006, **18**, 4259–4269.
43 M. S. Yuan, Q. Fang, Z. Q. Liu, J. P. Guo, H. Y. Chen, W. T. Yu, G. Xue and D. S. Liu, *J. Org. Chem.*, 2006, **71**, 7858–7861.
44 J. L. Wang, J. Luo, L. H. Liu, Q. F. Zhou, Y. G. Ma and J. Pei, *Org. Lett.*, 2006, **8**, 2281–2284.
45 S. C. Yuan, Q. J. Sun, T. Lei, B. Du, Y. F. Li and J. Pei, *Tetrahedron*, 2009, **65**, 4165–4172.
46 J. Luo, Y. Zhou, Z. Q. Niu, Q. F. Zhou, Y. G. Ma and J. Pei, *J. Am. Chem. Soc.*, 2007, **129**, 11314–11315.
47 L. Yao, S. H. Sun, S. F. Xue, S. T. Zhang, X. Y. Wu, H. H. Zhang, Y. Y. Pan, C. Gu, F. H. Li and Y. G. Ma, *J. Phys. Chem. C*, 2013, **117**, 14189–14196.
48 T. Karstens and K. Kobs, *J. Phys. Chem.*, 1980, **84**, 1871–1872.
49 J. Pomrnerehne, H. Vestweber, W. Guss, R. F. Muhrt, H. Bässler, M. Porsch and J. Daub, *Adv. Mater.*, 1995, **7**, 551–554.
50 W. R. Wadt and P. J. Hay, *J. Chem. Phys.*, 1985, **82**, 284–298.
51 P. J. Hay and W. R. Wadt, *J. Chem. Phys.*, 1985, **82**, 299–310.
52 Z. L. Cai and J. R. Reimers, *J. Phys. Chem. A*, 2000, **104**, 8389–8408.
53 R. Guan, Y. H. Xu, L. Ying, W. Yang, H. B. Wu, Q. L. Chen and Y. Cao, *J. Mater. Chem.*, 2009, **19**, 531–537.
54 A. Iraqi and I. Wataru, *Chem. Mater.*, 2004, **16**, 442–448.
55 I. Avilov, P. Marsal, J. L. Bredas and D. Beljonne, *Adv. Mater.*, 2004, **16**, 1624–1629.
56 P. Moonsin, N. Prachumrak, S. Namuangruk, S. Jungsuttiwong, T. Keawin, T. Sudyoadsuk and V. Promarak, *J. Mater. Chem. C*, 2014, **2**, 5540–5552.
57 E. Peeters, A. M. Ramos, S. C. J. Meskers and R. A. J. Janssen, *J. Chem. Phys.*, 2000, **112**, 9445–9454.
58 T. Forster and K. Kasper, *Z. Phys. Chem.*, 1954, **1**, 275–277.

